Konya Mühendislik Bilimleri Dergisi, c. 12, s. 2, 451-464, 2024
Konya Journal of Engineering Sciences, v. 12, n. 2, 451-464, 2024
ISSN: 2667-8055 (Electronic)
DOI: 10.36306/konjes.1402235

# THE INFLUENCE OF FUSED FILAMENT FABRICATION PARAMETERS ON THE FRACTURE BEHAVIOR OF PLA SPECIMENS CONSIDERING ENERGY CONSUMPTION

[1,*] Osman ÖZTÜRK, [2] Muhammed Arif ŞEN, [3] Mevlüt AYDIN

*Konya Technical University, Engineering and Natural Sciences Faculty, Mechanical Engineering Department, Konya, TÜRKİYE*

[1] osmanozturk@ktun.edu.tr, [2] masen@ktun.edu.tr, [3] maydin@ktun.edu.tr

## *Highlights*

- Quasi-static penetration test of the 3D printed polylactic acid (PLA) specimens.
- Exploration of role of the printing parameters on the fracture behavior.
- CPA optimization algorithm was used for maximum fracture force and reasonable power usage.

## *Graphical Abstract*

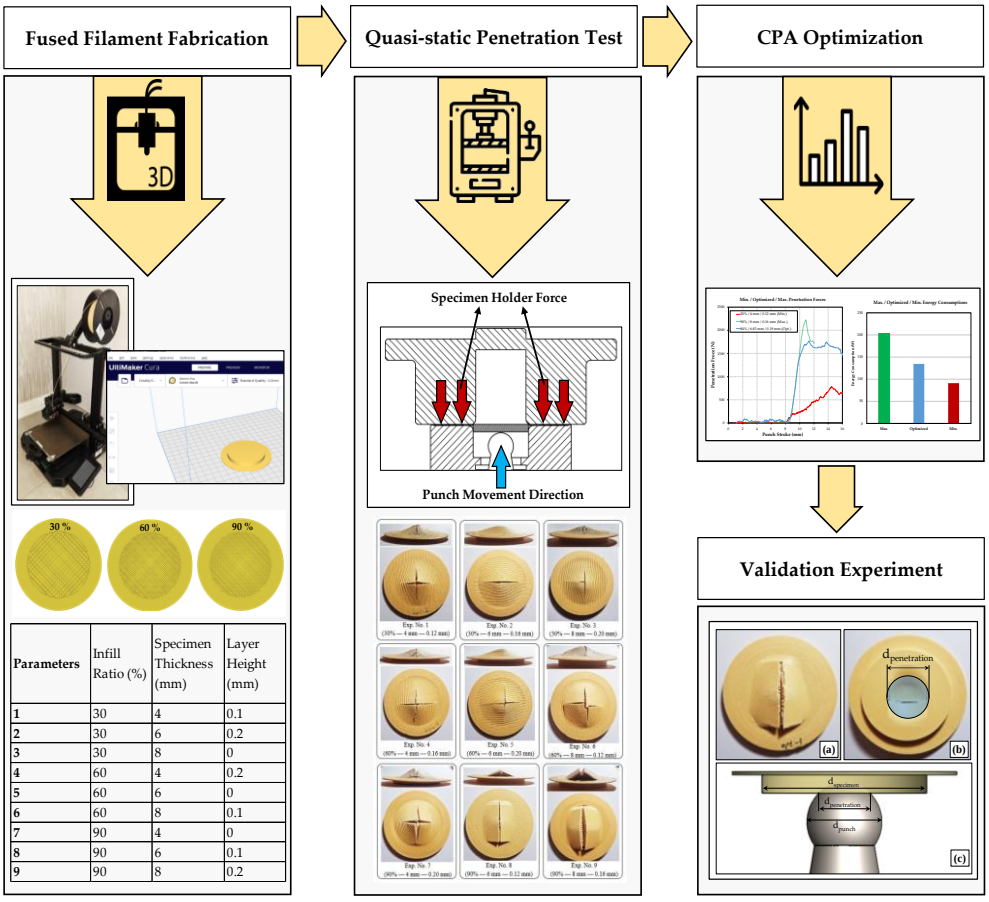


| Parameters | Infill Ratio (%) | Specimen Thickness (mm) | Layer Height (mm) |
|---|---|---|---|
| 1 | 30 | 4 | 0.1 |
| 2 | 30 | 6 | 0.2 |
| 3 | 30 | 8 | 0 |
| 4 | 60 | 4 | 0.2 |
| 5 | 60 | 6 | 0 |
| 6 | 60 | 8 | 0.1 |
| 7 | 90 | 4 | 0 |
| 8 | 90 | 6 | 0.1 |
| 9 | 90 | 8 | 0.2 |

*Corresponding Author: Osman ÖZTÜRK, osmanozturk@ktun.edu.tr

Konya Mühendislik Bilimleri Dergisi, c. 12, s. 2, 451-464, 2024
Konya Journal of Engineering Sciences, v. 12, n. 2, 451-464, 2024
ISSN: 2667-8055 (Electronic)
DOI: 10.36306/konjes.1402235

# THE INFLUENCE OF FUSED FILAMENT FABRICATION PARAMETERS ON THE FRACTURE BEHAVIOR OF PLA SPECIMENS CONSIDERING ENERGY CONSUMPTION

[1,*] Osman ÖZTÜRK, [2] Muhammed Arif ŞEN, [3] Mevlüt AYDIN

*Konya Technical University, Engineering and Natural Sciences Faculty, Mechanical Engineering Department, Konya, TÜRKİYE*

[1] osmanozturk@ktun.edu.tr, [2] masen@ktun.edu.tr, [3] maydin@ktun.edu.tr

**(Received: 08.12.2023; Accepted in Revised Form: 01.04.2024)**

**ABSTRACT:** Fused Filament Fabrication (FFF) is a 3D (three-dimensional) printing technology that allows the production of polymers with a wide range of infill densities and unlimited geometric variations. Because of this flexibility, mechanical properties can be optimized by tuning printing parameters. However, the energy consumption during fabrication varies significantly for different printing settings. In the present study, both maximum fracture force and minimum energy consumption of 3D printed PLA (Polylactic Acid) are achieved together by optimizing the printing parameters using CPA (Cyclical Parthenogenesis Algorithm) optimization algorithm. Firstly, a quasi-static penetration test is performed to measure the maximum fracture force. The energy consumption of each specimen is also calculated. Then, maximum fracture force and energy consumption are modeled and integrated into the optimization algorithm. As a result, the three most convenient parameter levels are 84%, 6.83 mm, and 0.19 mm for infill ratio, specimen thickness, and layer height, respectively. While high infill ratio values and specimen thickness increase mechanical performance, these parameter levels are disadvantageous for energy consumption. As a result of optimization, parameters that provide balanced strength and energy consumption were obtained. Fracture force and energy consumption are 1829.87 N and 134.56 W, respectively for the validation experiment of the optimal solution.

***Keywords:*** *3D Printing, Additive Manufacturing, Fused Filament Fabrication, PLA, Quasi-Static Penetration, Optimization*

## 1. INTRODUCTION

Additive manufacturing processes enable the manufacture of complex parts more easily compared to traditional forming and manufacturing techniques [1]. Additive manufacturing is used in industry with various techniques such as stereolithography [2], selective laser melting [3], and fused filament fabrication [4]. Among these methods, Fused Filament Fabrication (FFF), is an additive manufacturing method primarily based on the deposition of extruded filament layers for a complex 3D geometry. FFF printers have recently become the most popular machines for the printing of polymers because the printed complex parts can be produced and revised easily with a considerably low-cost printing machine [5]. There are many parameters in FFF, and parameter selection affects mechanical properties such as tensile or compressive strength. The influence of parameters is not limited to mechanical properties. Printing parameters also highly influenced the dimensional accuracy [6] and surface quality [7]. In addition to product quality, the energy consumption of FFF printers significantly depends on the printing settings. Therefore, various printing settings such as layer height, infill ratio, infill pattern, build orientation, printing temperature, and printing speed are investigated in the literature [8]. The influence of these parameters on the process was investigated for commonly used thermoplastic materials such as Polylactic acid (PLA), Acrylonitrile butadiene styrene (ABS), and Polyethylene terephthalate-glycol (PETG). Among these alternatives, PLA is a biodegradable filament material because PLA is obtained from crops such as corn and sugar beet. ABS is more durable but less eco-friendly. PETG is suitable for products in contact with food and beverages, but PETG is the least durable material among other alternatives. Because PLA

***Corresponding Author**: Osman ÖZTÜRK, osmanozturk@ktun.edu.tr

is biodegradable and ideal for prototype manufacturing, automotive, packaging, and prosthesis applications; PLA is the most popular material, which is an alternative to petroleum-based polymer materials [9]. The studies related to influence of parameters are focused on effect of layer thickness [10, 11], infill ratio [12] and raster orientation [13] etc.

Optimization of 3D printing parameters is widely investigated in academic and industrial studies. In a study aiming to minimize printing time and to optimize printing parameters, the most suitable infill type, infill ratio and layer height for PLA material was determined [14]. The best parameters for the minimum printing time are found as grid, 300 μm and 10% for the infill type, layer height and infill ratio respectively. In a study conducted by Korkut et al. [15], the effect of bed temperature, layer height, printing speed and nozzle temperature are found as the most significant variables considering reasonable printing time and lower energy consumption. The results indicate a decrease of 6.91% in energy usage and a considerable shortening in printing time. Kamer et al. [16] compared two different printers and two filaments with different thicknesses (1.75 mm and 2.85 mm) were compared in terms of energy consumption before, during and after printing a standard tensile test specimen. The most important result was that the power usage per specimen was considerably reduced when multiple test specimens were printed instead of printing specimens one by one. Şirin et al. [17] investigated the wear behavior of the 3D printed PLA materials with different infill densities. The results indicate that the wear performance of the middle level of infill density (50%) is better than high and low-level infill densities (70% and 30%, respectively). Akıncıoğlu et al. [18] performed friction tests of Acrylonitrile Styrene Acrylate (ASA) filament by using pin on disc test setup. One of the most significant results of this study is that the wear characteristic of the ASA depends highly on the surface quality and contact area, which also depends on infill density. The effect of different infill ratios on the wear properties of ABS was studied by Akıncıoğlu et al. by using a pin-on-disc device [19]. It was clearly emphasized that higher the infill density higher the coefficient of friction and friction temperature. The wear characteristics of cylindrical and flexible 3D printed scaffolds are also investigated by researchers [20]. As an overall result, studies on the mechanical and wear properties of 3D printed polymeric materials remain up-to-date and continue intensively.

In this study, the fracture forces of PLA samples produced by FFF were determined by quasi-static penetration test. The different printing parameters are investigated and optimized using CPA. These parameters are three various infill ratios (30%, 60%, 90%), specimen thickness (4 mm, 6 mm, and 8 mm), and layer height (0.12 mm, 0.16 mm, and 0.20 mm) which were used when manufacturing the test specimens. The fractured specimens were pictured prior to and after the test to illustrate the fracture patterns. The novelty of the current work is using quasi-static penetration test to reveal fracture behavior considering energy consumption in the 3D printing phase. The secondary purpose is to optimize the printing parameters for higher fracture force and lower energy consumption using CPA.

## 2. MATERIAL AND METHODS

### 2.1. Experimental Method

This study aims to reveal the effect of infill ratio, specimen thickness, and layer height on the fracture behavior of PLA material. The specimen was printed by Creality Ender3 S1 Pro printing machine using a 1.75 mm wood colored Esun PLA+ filament. The technical specifications of Creality Ender3 S1 Pro and Esun PLA+ filament are given in Table 1 [21, 22]. The melting point of the commercial Esun PLA+ filament is stated generally as 170-180 °C for PLA in the literature where some of the results are supported by DSC (Differential Scanning Calorimetryanalyses) [23, 24]. To avoid the other influencing factors; the built orientation, printing position, infill pattern, printing temperature, and printing speed were set as constant for all specimens. These fixed parameters are given in Table 2 with their values. Infill pattern was chosen as grid, a commonly used pattern for general applications. Infill ratio is crucial for strength, and layer height significantly reduces printing time. While the total thickness of the specimen is irrelevant from 3D printing settings, thickness affects the fracture force of the PLA material. Therefore, infill ratio (30%, 60%, 90%), specimen thickness (4 mm, 6 mm, 8 mm), and layer height (0.12 mm, 0.16 mm, 0.20 mm) are chosen

as the input parameters of this study. The printing machine and parameters intended to be optimized are given in Figure 1. The filament in this study is a wood colored filament which is a thermoplastic material used in 3D printing.

**Table 1.** The technical specifications of Creality Ender 3 S1 Pro 3D printing machine and Esun PLA+ filament

| Creality Ender 3 S1 Pro | | | Esun PLA+ | | |
|---|---|---|---|---|---|
| **Parameter** | **Value** | **Unit** | **Parameter** | **Value** | **Unit** |
| Build Volume | 220x220x270 | mm | Tensile Strength | 63 | MPa |
| Printing Speed | Up to 160 | $mm \cdot s^{-1}$ | Elongation at break | 20 | % |
| Printing Precision | ±0.1 | mm | Density | 1.23 | $g/cm^3$ |
| Layer Height | 0.1-0.35 | mm | Melting Point | 170-180 | °C |
| Filament Diameter | 1.75 | mm | Diameter | 1.75 | mm |
| Nozzle Diameter | 0.4 | mm | | | |
| Nozzle Temperature | Up to 300 | °C | | | |
| Bed Temperature | Up to 110 | °C | | | |
| Rated Power | 350 | W | | | |
| Supported Filament | PLA, ABS, TPU, PETG, PA | — | | | |

**Table 2.** Fixed 3D printing parameters

| **Parameter** | **Value** | **Unit** |
|---|---|---|
| Printing Speed | 70 | $mm \cdot s^{-}$ |
| Nozzle Temperature | 210 | °C |
| Bed Temperature | 60 | °C |
| Top Layer Thickness | 1 | mm |
| Bottom Layer Thickness | 1 | mm |
| Infill Pattern | GRID | — |
| Wall Thickness | 0.8 | mm |
| Wall Line Count | 2 | — |

A systematic approach was preferred to reduce the number of experiments. Instead of a full factorial design, the Taguchi design of experiment by L9 orthogonal array, which is given in Table 3, was used in this study. Taguchi L9 design is generally used in the literature to estimate the factors that influence the mechanical performance of the printed part and which factors are more significant than others [25]. The CAD (Computer Aided Design) model of the test specimen was designed considering its thickness, as the specimen thickness is one of the parameters in this study. After that, the designed models were imported to slicing software Ultimaker Cura (version 5.3.1) so that the infill ratio and layer height were set to the required values in Table 3. In the next step, the G-code of the sliced models were uploaded to the 3D-printer and the test samples were ready to be printed. The printing stages of the samples are given in Figure 2.

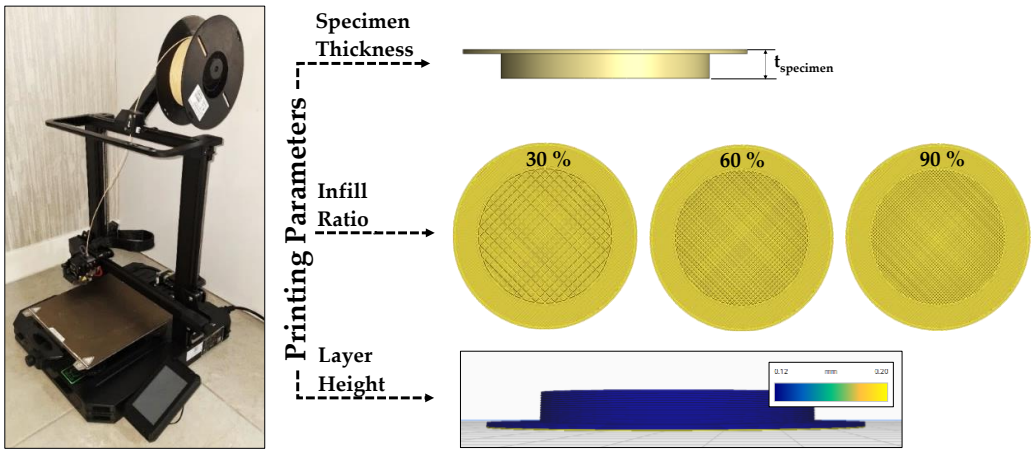


**Figure 1.** Creality Ender 3 S1 Pro 3D Printer and printing parameters (specimen thickness, infill ratio, layer height)

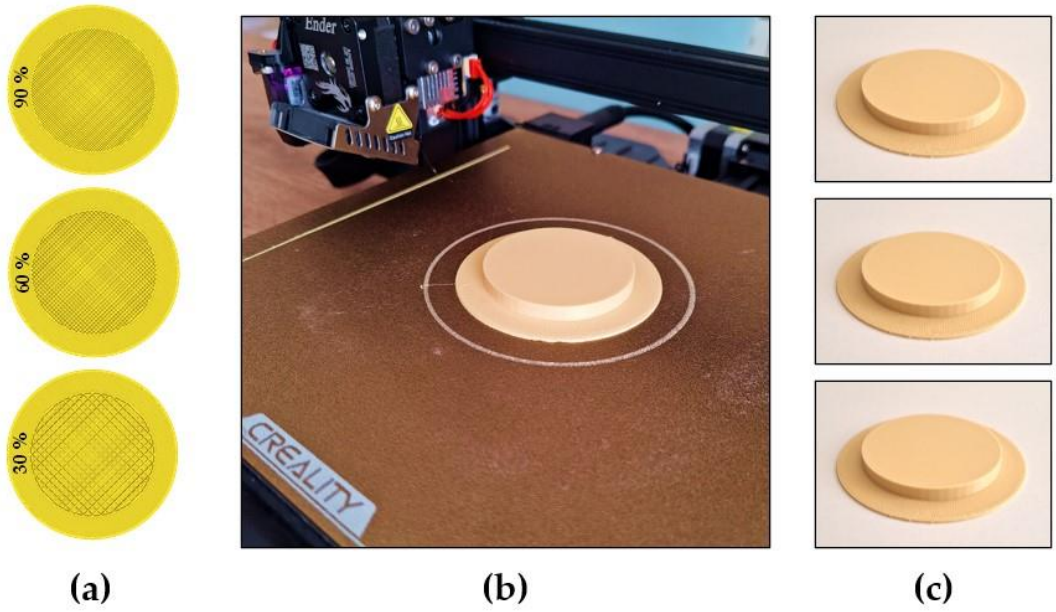


**Figure 2.** (a) Sliced specimen models in Ultimaker Cura 5.3.1, (b) printing one specimen at a time, (c) final printed specimens

**Table 3.** The experimental design according to Taguchi L9 and the variables (specimen thickness and printing parameters)

| **Parameters** | **1** | **2** | **3** | **4** | **5** | **6** | **7** | **8** | **9** |
|---|---|---|---|---|---|---|---|---|---|
| Infill Ratio (%) | 30 | 30 | 30 | 60 | 60 | 60 | 90 | 90 | 90 |
| Specimen Thickness (mm) | 4 | 6 | 8 | 4 | 6 | 8 | 4 | 6 | 8 |
| Layer Height (mm) | 0.1 | 0.2 | 0 | 0.2 | 0 | 0.1 | 0 | 0.1 | 0.2 |

After all specimens were printed, quasi-static penetration tests were performed in a four-column hydraulic press. In the penetration test, two dies were used. The diameters of the upper and lower dies are 50 mm and 55 mm, respectively. The dimensions of the specimen were chosen to be compatible with

standard quasi-static testing. In the literature, the ratio between the die cavity diameter and the punch head diameter ($D_{cavity}/D_{punch}$) is defined as 'SPR', a value which must be in the range of 1.01<SPR<13.33 [26]. In this study, the diameter of the semi-spherical punch is 24 mm, and the diameter of the die cavity is 50 mm. Therefore, SPR of this study is 2.08 which is acceptable for the quasi-static penetration test. The specimen was designed with a 1 mm brim at the bottom so the specimen holder force could be applied without damaging the main specimen. During each penetration experiment, penetration forces in response to punch stroke were recorded with WinView software. The exploded, sectional, and literal views of the test are given in Figure 3a, 3b and 3c respectively. The working principle of the test is given in sectional view in Figure 3b. The fracture force of the specimen was determined by the first significant drop in the penetration force. In addition, the energy consumption was determined using a smart watt-meter during the 3D printing process. Total printing time and instantaneous energy utilization were used to measure each specimen's energy consumption.

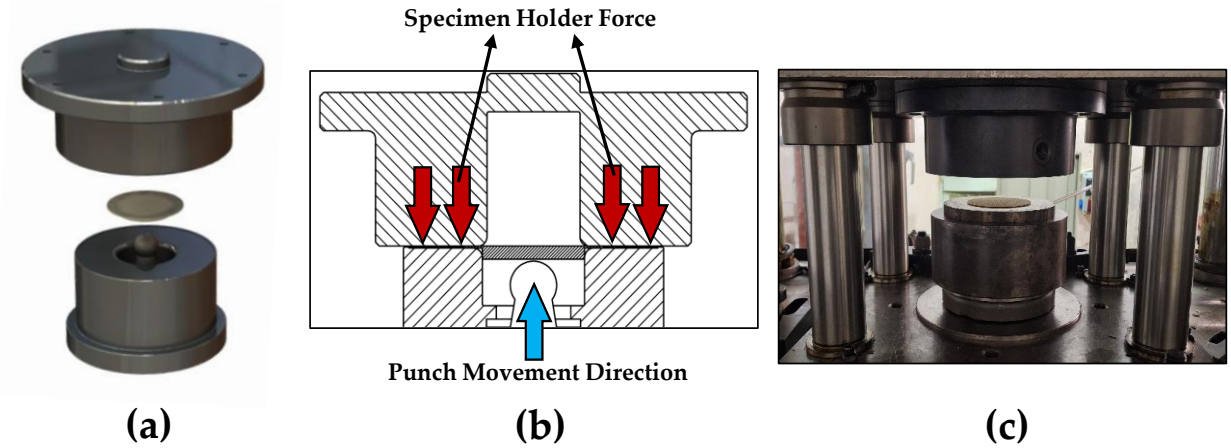


**Figure 3.** (a) Exploded view, (b) sectional view and (c) literal view of the experimental setup for Quasi-static Penetration Test

### 2.2. Modeling and Optimization

This section describes the obtaining of mathematical modeling by the experimental dataset and later tuned printing parameters using a metaheuristic algorithm via the model. Generating a mathematical expression of all FFF parameters can be challenging and possibly impossible. However, it is a very efficient and effective method to develop mathematical formulations that can accurately represent the process with sufficient experimental data.

As can be seen in the below equations, the quasi-static penetration test data of samples produced with the FFF were modeled in Minitab software where the inputs are three main parameters (infill ratio, specimen thickness, and layer height), and the outputs are fracture force and energy consumption, separately. The second-degree polynomial equations giving the mathematical relationship between the printing parameters and fracture force (Eq.1) and energy consumption (Eq. 2) are obtained as follows.

$$y_1 = -2178 - [65.20 \cdot x_1] + [955 \cdot x_2] + [23416 \cdot x_3] + [0.3293 \cdot {x_1}^2] - [56.01 \cdot {x_2}^2] - [120792 \cdot {x_3}^2] - [0.099 \cdot x_1 \cdot x_2] + [221.2 \cdot x_1 \cdot x_3] \quad (1)$$

$$y_2 = 509.7 + [1.308 \cdot x_1] + [28 \cdot x_2] - [6115 \cdot x_3] - [0.00623 \cdot {x_1}^2] - [1.402 \cdot {x_2}^2] + [16207 \cdot {x_3}^2] \quad (2)$$

In these equations; $x_1$, $x_2$, and $x_3$ are infill ratio, specimen thickness, and layer height, respectively. All coded variables and parameter ranges are given in Table 4. Table 4 is an explanation of how input and output variables are expressed in the objective function. For example, the parameter "infill ratio" is

represented as $x_1$ in the objective function. Additionally, the range in which these parameters will be optimized must be defined as a constraint in the CPA. For this reason, the most used range in the literature was chosen for the input parameters and is given in Table 4. For example, the parameter range for infill ratio is $30 \geq x_1 \geq 90$, so the optimization will be performed within this range. Using these mathematical formulations, the optimal infill ratio, specimen thickness, and layer height values that can provide the highest strength, maximum fracture force, despite as less energy consuming as possible in the FFF process, are tunned with the CPA.

**Table 4.** Coded variables and preferred parameter ranges in 3D printing

| **Input Parameters** | **Coded Variables** | **Unit** | **Parameter Range** |
|---|---|---|---|
| Infill Ratio | $x_1$ | % | $30 \geq x_1 \geq 90$ |
| Specimen Thickness | $x_2$ | mm | $4 \geq x_2 \geq 8$ |
| Layer Height | $x_3$ | mm | $0.12 \geq x_3 \geq 0.2$ |
| **Output Parameters** | **Coded Variables** | **Unit** | |
| Fracture Force | $y_1$ | N | |
| Power Consumption | $y_2$ | W | |

CPA optimization method is one of the newly introduced heuristic optimization methods. Firstly, proposed by Kaveh and Zolghadr in 2017, Cyclical Parthenogenesis Algorithm (CPA) is a population-based metaheuristic search algorithm [27]. CPA is developed by inspiring social behavior and the reproduction of aphids which is a kind of zoological organism. The sexual and asexual reproduction abilities of aphids, named cyclical parthenogenesis, and some unique aspects of their life are exciting for many optimization approaches. CPA is successfully applied to solve many optimization problems. As with all population-based algorithms, CPA starts with a randomly generated aphid population, which includes candidate solutions. Each iteration runs along a five-step and evaluates the objective function according to the newly generated candidate solutions. Detailed descriptions and pseudocode of CPA are available in the literature [28, 29, 30].

The objective function ($J$) that is determined to maximize the Fracture Force ($F_f$) while minimizing the energy consumption ($E_C$) is given in Equation 3. Here, $c_1$ and $c_2$ are used to weigh the components in the objective function because fracture force and energy consumption are different physical values with dissimilar units. The constant gains $c_1$ and $c_2$ are determined as 112.14 and 1693.07, respectively.

$$J = \left(c_1 F_f\right) * \left(c_2 E_C\right)^{-1} \tag{3}$$

## 3. RESULTS AND DISCUSSION

### 3.1. Experimental Results

The results of the penetration test are given in Figure 4. According to the test results, the fracture directions were generally in two directions, and these directions were perpendicular to each other. The fracture characteristic is brittle, similar to the literature [31]. As expected, as the specimen thickness and infill ratio increased, the force at which the fracture started also increased. The penetration force was measured instantly throughout the test, and the force value at which the fracture started was taken as fracture force. Penetration and fracture forces are given in Figure 5.

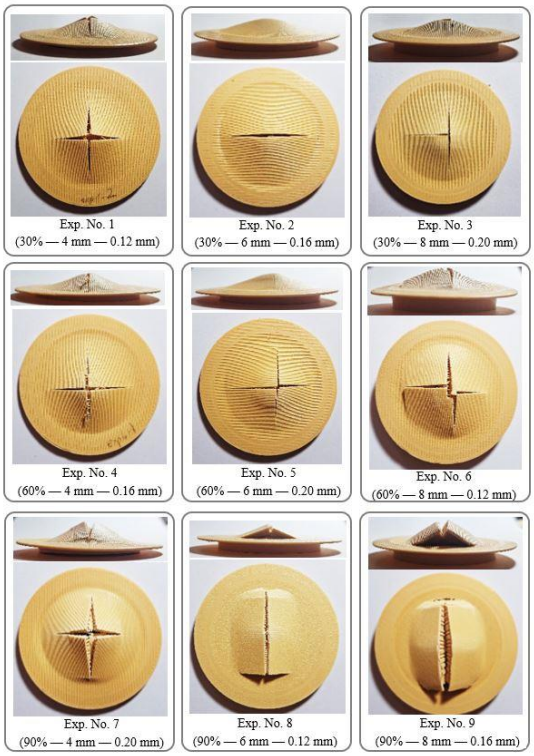


**Figure 4.** Experimental results of the quasi-static penetration test

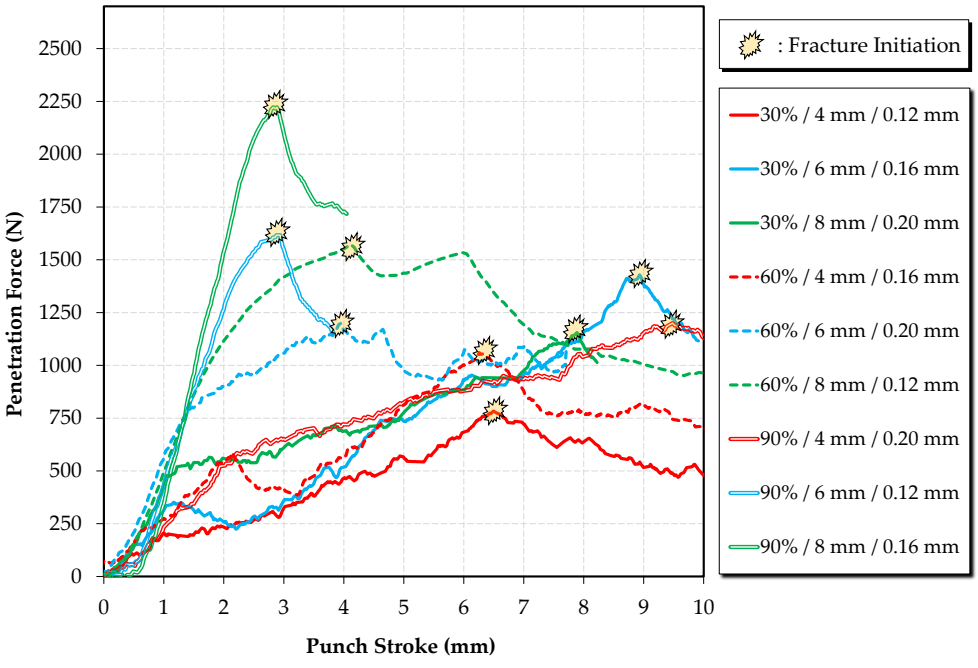


**Figure 5.** The results of the penetration force versus punch stroke and fracture initiation points

### 3.2. Optimization Results

The ideal CPA parameters were assigned as 20, 2, 0.02, 0.03, and 0.7 for nA, nC, step size ($\alpha_1$), step size ($\alpha_2$), and Fr, respectively, using a trial-and-error method. As it can be clearly understood in Table 5, to define every CPA parameter, each parameter value was defined as minimizing the objective function by

keeping the others constant.

After constructing the mathematical equations, objective function, and CPA in MATLAB R2022b, the algorithm was run to search for optimal infill ratio, specimen thickness, and layer height values, which ensure the best fit of the transfer function. The printing parameters, which could ensure that the maximum fracture force with reasonable energy consumption, were optimized. These are given in Table 5 in bold.

The optimum algorithm parameters of the CPA were found using the trial-and-error method, as explained in detail before. Using these parameters, the algorithm has been run more than once. Printing parameters that minimize the fit function are given in the first row of Table 6, which is the best run in this case. The convergence graph for minimum, maximum, and mean values is given in Figure 6.

**Table 5.** Finding the best optimization parameter by ranking the value of the fit function

| No. | nA | $x_1$ (Infill Ratio) | $x_2$ (Specimen Thickness) | $x_3$ (Layer Height) | Fit | Rank |
|---|---|---|---|---|---|---|
| 1-1 | 10 | 86.990 | 7.922 | 0.192 | 0.853 | 5 |
| 1-2 | 15 | 89.529 | 5.886 | 0.184 | 0.833 | 2 |
| **1-3** | **20** | **90.000** | **6.659** | **0.180** | **0.817** | **1** |
| 1-4 | 25 | 89.869 | 7.216 | 0.174 | 0.833 | 3 |
| 1-5 | 30 | 87.306 | 6.539 | 0.191 | 0.848 | 4 |
| | **nC** | | | | | |
| **2-1** | **2** | **90.000** | **7.114** | **0.180** | **0.82** | **1** |
| 2-2 | 3 | 78.751 | 6.284 | 0.171 | 0.97 | 5 |
| 2-3 | 4 | 80.052 | 7.561 | 0.174 | 0.92 | 4 |
| 2-4 | 5 | 87.192 | 5.961 | 0.182 | 0.86 | 3 |
| 2-5 | 6 | 90.000 | 7.699 | 0.191 | 0.82 | 2 |
| | **Stepsize** | | | | | |
| 3-1 | $\alpha_1$:0.01 $\alpha_2$:0.01 | 86.831 | 7.643 | 0.191 | 0.85 | 7 |
| 3-2 | $\alpha_1$:0.01 $\alpha_2$:0.02 | 86.429 | 7.148 | 0.181 | 0.85 | 6 |
| 3-3 | $\alpha_1$:0.01 $\alpha_2$:0.03 | 87.404 | 5.566 | 0.172 | 0.9 | 9 |
| 3-4 | $\alpha_1$:0.02 $\alpha_2$:0.01 | 88.508 | 6.961 | 0.189 | 0.83 | 4 |
| 3-5 | $\alpha_1$:0.02 $\alpha_2$:0.02 | 86.514 | 7.197 | 0.192 | 0.85 | 8 |
| **3-6** | **$\alpha_1$:0.02 $\alpha_2$:0.03** | **90.000** | **7.322** | **0.187** | **0.81** | **1** |
| 3-7 | $\alpha_1$:0.03 $\alpha_2$:0.01 | 90.000 | 6.543 | 0.186 | 0.81 | 2 |
| 3-8 | $\alpha_1$:0.03 $\alpha_2$:0.02 | 90.000 | 5.975 | 0.187 | 0.82 | 3 |
| 3-9 | $\alpha_1$:0.03 $\alpha_2$:0.03 | 88.918 | 7.951 | 0.189 | 0.83 | 5 |
| | **Fr** | | | | | |
| 4-1 | 0.2 | 90.000 | 7.733 | 0.165 | 0.878 | 6 |
| 4-2 | 0.3 | 90.000 | 5.529 | 0.181 | 0.843 | 5 |
| 4-3 | 0.4 | 90.000 | 6.349 | 0.185 | 0.816 | 4 |
| 4-4 | 0.5 | 78.492 | 6.266 | 0.172 | 0.965 | 7 |
| 4-5 | 0.6 | 90.000 | 6.399 | 0.187 | 0.815 | 3 |
| **4-6** | **0.7** | **90.000** | **7.009** | **0.184** | **0.810** | **1** |
| 4-7 | 0.8 | 90.000 | 7.167 | 0.188 | 0.810 | 2 |

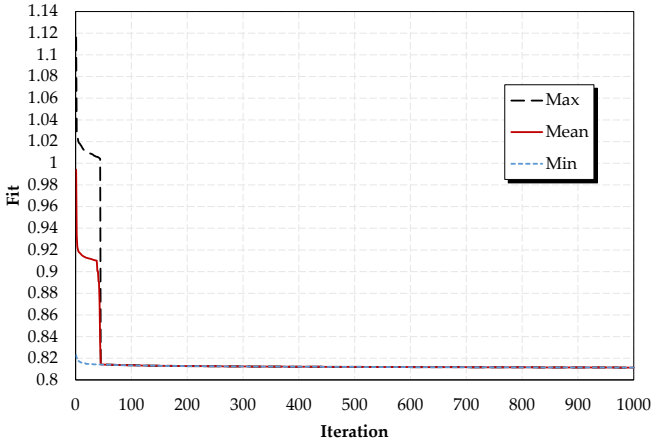


**Figure 6.** Convergence graph of the best optimization run

**Table 6.** The optimization algorithm was run several times for optimized printing parameters. Optimized parameters for the best fit (given bold in first row) are; 84%, 6.83 mm, 0.19 mm for $x_1$, $x_2$ and $x_3$ respectively

| $x_1$ (Infill Ratio) | $x_2$ (Specimen Thickness) | $x_3$ (Layer Height) | Fit | Rank |
|---|---|---|---|---|
| **83.77** | **6.83** | **0.19** | **0.812** | **1** |
| 87.54 | 6.22 | 0.18 | 0.861 | 4 |
| 88.85 | 7.62 | 0.19 | 0.828 | 2 |
| 88.64 | 5.29 | 0.17 | 0.912 | 6 |
| 89.22 | 7.37 | 0.16 | 0.858 | 3 |
| 90.00 | 6.84 | 0.19 | 0.884 | 5 |

The outputs obtained from the polynomial model and experimental outputs are given in Table 7. Both polynomial models developed for force and energy showed excellent agreement with the experimental results. The 10th row in Table 7 indicates the validation experiment results, which is the optimized solution for this study. The mathematical models are also good enough to predict the optimized output responses. The graphical representations of the fracture force and energy consumption are given in Figure 7 and Figure 8, respectively. As the graph implies, the fracture force is very close to the maximum value within the response space, while the energy consumption is near the average value. As a result, CPA can predict one of the optimal printing parameters with the aim of maximum fracture force and minimum energy consumption.

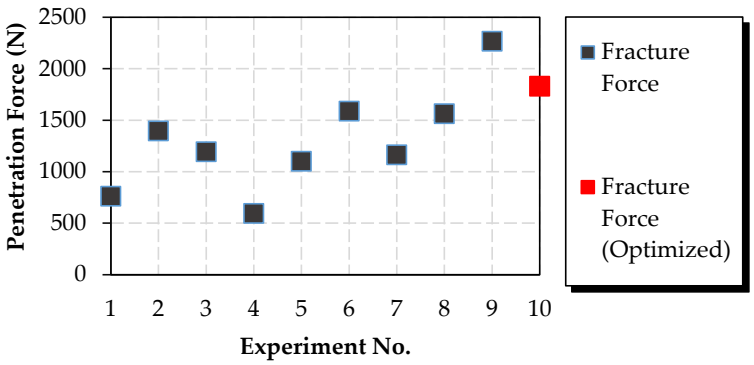


**Figure 7.** Comparison of optimized fracture force and corresponding Taguchi experiments

**Table 7.** The results of the Taguchi L9 orthogonal array and optimal solution. The results of the optimal solution (validation experiment) is given in 10th row in bold

| | Input Parameters | | | Output Responses (intended to be optimized) | | Output Responses | | Mathematical Model | |
|---|---|---|---|---|---|---|---|---|---|
| **Exp. No** | **Infill Ratio (%)** | **Specimen Thickness (mm)** | **Layer Height (mm)** | **Fracture Force (N)** | **Total energy consumption (Watt)** | **Printing Time (min)** | **Filament Consumption (g)** | **Fracture Force (N)** | **Total energy consumption (Watt)** |
| **1** | 30 | 4 | 0.12 | 763.25 | 130.36 | 93 | 11 | 761.17 | 132.48 |
| **2** | 30 | 6 | 0.16 | 1397.15 | 100.92 | 72 | 13 | 1394.23 | 97.36 |
| **3** | 30 | 8 | 0.2 | 1196.40 | 102.32 | 73 | 15 | 1192.69 | 102.89 |
| **4** | 60 | 4 | 0.16 | 595.65 | 91.11 | 65 | 12 | 593.36 | 91.82 |
| **5** | 60 | 6 | 0.2 | 1102.55 | 106.53 | 76 | 16 | 1099.40 | 108.56 |
| **6** | 60 | 8 | 0.12 | 1590.40 | 203.24 | 145 | 20 | 1586.48 | 199.60 |
| **7** | 90 | 4 | 0.2 | 1165.15 | 95.31 | 68 | 14 | 1162.65 | 91.81 |
| **8** | 90 | 6 | 0.12 | 1564.30 | 193.43 | 138 | 19 | 1560.99 | 194.07 |
| **9** | 90 | 8 | 0.16 | 2269.15 | 145.77 | 104 | 24 | 2264.97 | 147.73 |
| **10** | **84** | **6.83** | **0.19** | **1829.87** | **134.56** | **96** | **21** | **1960.59** | **124.67** |

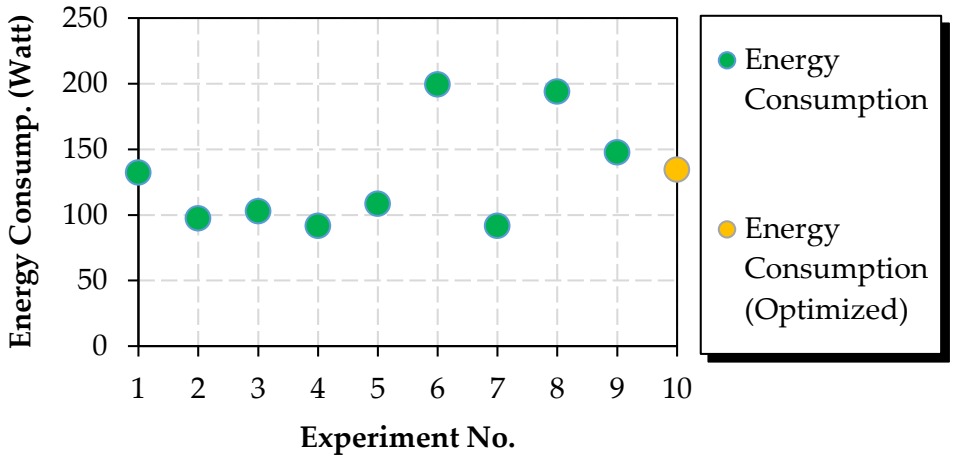


**Figure 8.** Comparison of optimized energy consumption and corresponding Taguchi experiments

Finally, the graphs of penetration force versus punch stroke are given in Figure 9a. These graphs compare the minimum and maximum fracture forces of Taguchi experiments with the optimal solution. The corresponding energy utilizations are also provided in Figure 9b. Judging by the result, the fracture force improved significantly, while the energy consumption of the optimal specimen remained approximately in the middle of Taguchi experiments.

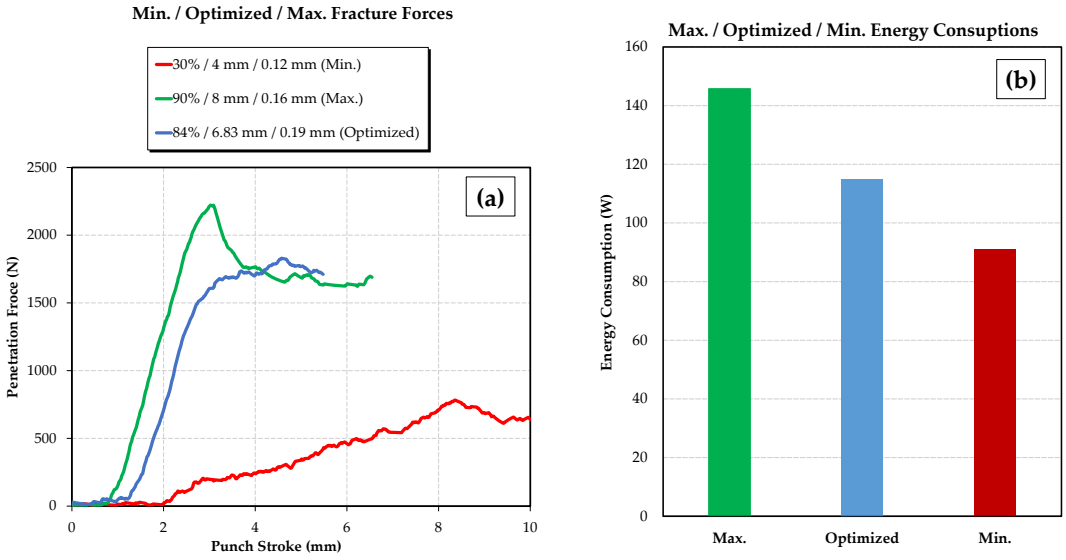


**Figure 9.** (a) Minimum, maximum, and optimal fracture forces, (b) maximum, minimum and optimal energy consumptions

### 3.3. Validation Experiment

A validation experiment was performed after optimization. A characteristic penetration behavior is given in Figure 10a, 10b and 10c. As the figures imply, the material appears to fail before full penetration of the material. The reason behind this phenomenon is the damage mechanism by penetration consists of various damage shapes as stated in previous studies in the literature [32]. The damage mechanism began with small sized cracks near the area that is in contact with the spherical punch. The damage proceeded with either cross shaped or linear shaped larger cracks. Eventually the material was completely damaged. Both the linear and the cross shaped cracks were mainly the result of excessive shear stresses in the grid structure of the PLA.

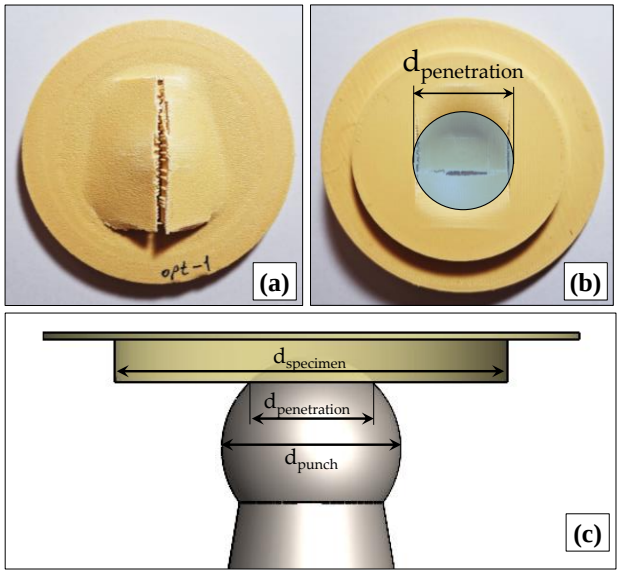


**Figure 10.** (a) Front view, (b) back view of the fractured specimen and (c) comparison of the penetration and punch diameters at failure

## 4. CONCLUSIONS

In this study, to improve the maximum fracture of 3D printed PLA materials with minimum energy consumption on Fused Filament Fabrication, which is a current and developing manufacturing method, the optimal printing parameters (infill ratio, specimen thickness, and layer height) are adjusted using metaheuristic CPA.

When the results obtained from modeling and experimental studies were examined, it was understood that the proposed method could successfully adjust the printer parameters to provide the desired objective function. The optimum parameters of the CPA were obtained by trial-and-error method. The CPA has performed well in providing 3D printing parameters that provide the highest fracture force and lowest energy consumption when producing the part. It was observed that the sample produced with optimal parameters (84%, 6.83 mm and 0.19 mm for infill ratio, specimen thickness and layer height) could provide an energy consumption of 134.56 watts at an average value despite an above-average breaking force of 1829.87 N. This result indicates that an unlimited number of geometries can potentially be optimized for better impact performance while maintaining minimum energy usage. To gain a deeper and systematic understanding of fracture behavior of optimized polymer materials, the Essential Work of Failure (EWF) method should be used in future studies [33].

### Declaration of Ethical Standards

The authors followed all ethical guidelines, including authorship, citation, data reporting, and publishing original research.

### Declaration of Competing Interest

The authors declare that they have no known competing financial interests or personal relationships that could have appeared to influence the work reported in this paper.

### Funding / Acknowledgements

This study is not funded by any institution or council.

### Data Availability

The data that support the finding of this study are available from the corresponding author.

## REFERENCES

[1] I. J. Solomon, P. Sevvel, and J. Gunasekaran, "A review on the various processing parameters in FDM," *Mater. Today Proc.*, vol. 37, no. Part 2, pp. 509–514, 2020, doi: 10.1016/j.matpr.2020.05.484.

[2] C. Liu, B. Qian, X. Liu, L. Tong, and J. Qiu, "Additive manufacturing of silica glass using laser stereolithography with a top-down approach and fast debinding," *RSC Adv.*, vol. 8, no. 29, pp. 16344–16348, 2018, doi: 10.1039/c8ra02428f.

[3] E. Aydoğan Güngör, "Production of Oxide Dispersion Strengthened Inconel 718 Alloys Using Conventional Powder Metallurgy and Additive Manufacturing Methods," *Konya J. Eng. Sci.*, vol. 8055, pp. 678–692, 2023, doi: 10.36306/konjes.1254946.

[4] S. Singh, G. Singh, C. Prakash, and S. Ramakrishna, "Current status and future directions of fused filament fabrication," *J. Manuf. Process.*, vol. 55, no. April, pp. 288–306, 2020, doi: 10.1016/j.jmapro.2020.04.049.

[5] C. Fonda, E. Canessa, and M. Zennaro, *Low-Cost 3D Printing for Science, Education and Sustainable Development*. 2013. [Online]. Available: http://sdu.ictp.it/3d/book.html [Accessed: Dec. 8, 2023]

[6] R. Mendricky and D. Fris, "Analysis of the accuracy and the surface roughness of fdm/fff

technology and optimisation of process parameters," *Teh. Vjesn.*, vol. 27, no. 4, pp. 1166–1173, 2020, doi: 10.17559/TV-20190320142210.

[7] J. Kechagias, D. Chaidas, N. Vidakis, K. Salonitis, and N. M. Vaxevanidis, "Key parameters controlling surface quality and dimensional accuracy: a critical review of FFF process," *Mater. Manuf. Process.*, vol. 37, no. 9, pp. 963–984, 2022, doi: 10.1080/10426914.2022.2032144.

[8] V. Cojocaru, D. Frunzaverde, C. O. Miclosina, and G. Marginean, "The Influence of the Process Parameters on the Mechanical Properties of PLA Specimens Produced by Fused Filament Fabrication—A Review," *Polymers (Basel).*, vol. 14, no. 5, pp. 886-909, 2022, doi: 10.3390/polym14050886.

[9] A. Pandzic, D. Hodzic, and A. Milovanovic, "Influence of carbon fibers on mechanical properties of materials in FDM technology," *Ann. DAAAM Proc. Int. DAAAM Symp.*, vol. 30, no. 1, pp. 545–554, 2019, doi: 10.2507/30th.daaam.proceedings.074.

[10] O. Luzanin, D. Movrin, V. Stathopoulos, P. Pandis, T. Radusin, and V. Guduric, "Impact of processing parameters on tensile strength, in-process crystallinity and mesostructure in FDM-fabricated PLA specimens," *Rapid Prototyp. J.*, vol. 25, no. 8, pp. 1398–1410, 2019, doi: 10.1108/RPJ-12-2018-0316.

[11] J. Giri, A. Chiwande, Y. Gupta, C. Mahatme, and P. Giri, "Effect of process parameters on mechanical properties of 3d printed samples using FDM process," *Mater. Today Proc.*, vol. 47, pp. 5856–5861, 2021, doi: 10.1016/j.matpr.2021.04.283.

[12] A. Alafaghani and A. Qattawi, "Investigating the effect of fused deposition modeling processing parameters using Taguchi design of experiment method," *J. Manuf. Process.*, vol. 36, no. October, pp. 164–174, 2018, doi: 10.1016/j.jmapro.2018.09.025.

[13] Ö. Bayraktar, G. Uzun, R. Çakiroğlu, and A. Guldas, "Experimental study on the 3D-printed plastic parts and predicting the mechanical properties using artificial neural networks," *Polym. Adv. Technol.*, vol. 28, no. 8, pp. 1044–1051, 2017, doi: 10.1002/pat.3960.

[14] F. Kartal, C. Nazlı, Z. Yerlikaya, F. Şimşek, and M. H. Çetin, "Yapım Zamanı için Erimiş Birikim Modelleme İşlem Parametrelerinin Optimizasyonu". *Int. J. 3D Print. Tech. Dig. Ind.*, vol. 2, no. 1, pp. 97-104, 2018, https://dergipark.org.tr/en/pub/ij3dptdi/issue/36075/404817

[15] V. Korkut, and H. Yavuz, "Açık-Kaynaklı 3B Yazıcılarda Enerji ve Zaman Gereksinimini Azaltmada Etkili Parametrelerin İncelenmesi." *J. Ins. Sci. Technol.*, vol. 12, no. 1, pp. 403-411, 2022, doi: 10.21597/jist.903159.

[16] M. S. Kamer, Ş. Temiz, and A. Kaya, "Determination of Energy Consumption During The Tensile Test Sample Production in 3D Printer Working with The Fused Deposition Modeling Method. *J. Inst. of Sci. Technol.*, vol. 13, no. 3, pp. 1998-2007, 2023, doi: 10.21597/jist.1198510.

[17] Ş. Şirin, E. Aslan, and & G. Akincioğlu, "Effects of 3D-printed PLA material with different filling densities on coefficient of friction performance,". *Rapid Prototyp. J.*, vol. 29, no. 1, pp. 157-165, 2023, doi: 10.1108/RPJ-03-2022-0081.

[18] G. Akıncıoğlu, and E. Aslan, "Investigation of tribological properties of amorphous thermoplastic samples with different filling densities produced by an additive manufacturing method," *Gazi Mühendislik Bilimleri Dergisi*, vol. 8, no. 3, pp. 540-546, 2021, doi: 10.30855/gmbd.0705041.

[19] G. Akıncıoğlu, E. Şirin, and E. Aslan, "Tribological characteristics of ABS structures with different infill densities tested by pin-on-disc," *Proc. Inst. Mech. Eng. J: J. Eng. Tribol.*, vol. 237, no. 5, pp. 1224-1234, 2023, doi: 10.1177/13506501231153521.

[20] E. Aslan, and G. Akincioğlu, "Tribological Characterization of Two Different Elastic Polymers Produced via FDM," *International Symposium on Lightweight and Sustainable Polymeric Materials*, pp. 189-200, 2023, doi: 10.1007/978-981-99-5567-1_14.

[21] "Ender 3 S1 Pro 3D Printer" [Online] Available: https://www.creality.com/products/creality-ender-3-s1-pro-fdm-3d-printer [Accessed Jan. 31, 2024]

[22] "ESUN PLA+ Technical Data Sheet" [Online] Available: https://www.esun3d.com/uploads/eSUN_PLA+-Filament_TDS_V4.0.pdf [Accessed Feb. 15, 2024]

[23] S. Yilmaz, B. Eyri, O. Gul, N.G. Karsli, and T. Yilmaz, (2024). "Investigation of the influence of salt remelting process on the mechanical, tribological, and thermal properties of 3D-printed poly (lactic acid) materials," *Polym. Eng. Sci.*, vol. 64, no.1, pp. 17-30, 2024, doi: 10.1002/pen.26526.

[24] H. Lara-Padilla, C. Mendoza-Buenrostro, D. Cardenas, A. Rodriguez-Garcia, and C.A. Rodriguez, "Influence of controlled cooling in bimodal scaffold fabrication using polymers with different melting temperatures," *Mater.*, vol. 10, no. 6, pp. 640, 2017, doi:10.3390/ma10060640.

[25] N. Lokesh, B. A. Praveena, J. Sudheer Reddy, V. K. Vasu, and S. Vijaykumar, "Evaluation on effect of printing process parameter through Taguchi approach on mechanical properties of 3D printed PLA specimens using FDM at constant printing temperature," *Mater. Today Proc.*, vol. 52, pp. 1288–1293, 2022, doi: 10.1016/j.matpr.2021.11.054.

[26] Ö.F. Erkendirci, and B.Z.G. Haque, "Quasi-static penetration resistance behavior of glass fiber reinforced thermoplastic composites," *Compos. B. Eng.*, vol. 43, no. 8, pp. 3391-3405, 2012, doi: 10.1016/j.compositesb.2012.01.053.

[27] A. Kaveh and A. Zolghadr, "Cyclical Parthenogenesis Algorithm: A new meta-heuristic algorithm," *Asian J. Civ. Eng.*, vol. 18, no. 5, pp. 673–701, 2017.

[28] A. Kaveh and A. Zolghadr, "Cyclical Parthenogenesis Algorithm for guided modal strain energy based structural damage detection," *Appl. Soft Comput. J.*, vol. 57, pp. 250–264, 2017, doi: 10.1016/j.asoc.2017.04.010.

[29] A. Kaveh and A. Zolghadr, "Optimal design of cyclically symmetric trusses with frequency constraints using cyclical parthenogenesis algorithm," *Adv. Struct. Eng.*, vol. 21, no. 5, pp. 739–755, 2018, doi: 10.1177/1369433217732492.

[30] A. Kaveh and A. Zolghadr, "Cyclical parthenogenesis algorithm for layout optimization of truss structures with frequency constraints," *Eng. Optim.*, vol. 49, no. 8, pp. 1317–1334, 2017, doi: 10.1080/0305215X.2016.1245730.

[31] S. Cicero, V. Martínez-Mata, L. Castanon-Jano, A. Alonso-Estebanez, and B. Arroyo, "Analysis of notch effect in the fracture behaviour of additively manufactured PLA and graphene reinforced PLA," *Theor. Appl. Fract. Mech.*, vol. 114, no. May, pp. 103032, 2021, doi: 10.1016/j.tafmec.2021.103032.

[32] P. Cheng, Y. Peng, K. Wang, A. Le Duigou, S. Yao, and C. Chen, "Quasi-static penetration property of 3D printed woven-like ramie fiber reinforced biocomposites". *Compos. Struct.*, vol. 303, 116313, 2023, doi: 10.1016/j.compstruct.2022.116313.

[33] I. I. Cuesta, E. Martinez-Pañeda, A. Díaz, and J. M. Alegre, (2019). "The Essential Work of Fracture parameters for 3D printed polymer sheets". *Mater. & Des.*, vol. 181, 107968, 2019, doi: 10.1016/j.matdes.2019.107968.